

Stochastic Absorption of the Light of Background Sources due to Intergalactic Neutral Hydrogen

I. Testing different line-number evolution models via the cosmic flux decrement

Thorsten Tepper-García¹* and Uta Fritze²

¹*Institut für Astrophysik, Georg-August Universität, Friedrich-Hund-Platz 1, D-37077 Göttingen*

²*Centre for Astrophysics Research, University of Hertfordshire, College Lane, Hatfield, AL10 9AB, UK*

Accepted —. Received —; in original form —.

ABSTRACT

We test the accuracy of different models of the attenuation of light due to resonant scattering by intergalactic neutral hydrogen by comparing their predictions of the evolution of the mean cosmic flux decrement D_A to measurements of this quantity based on observations. To this end, we use data available in the literature and our own measurements of the cosmic flux decrement for 25 quasi-stellar sources in the redshift range $2.64 < z_{em} < 5.41$ taken from the SDSS Data Release 5. In order to perform the measurements of D_A , we fit a power-law to the continuum redward of the Ly α emission line, and extrapolate this fit to region blueward of it, where the flux is severely affected by absorption due to intervening H α absorbers.

We compute, using numerical simulations, the redshift evolution of the mean flux depression, $D_A(z)$, due to the presence of Ly α Forest absorbers and Lyman limit systems randomly distributed along the line-of-sight, and compute its intrinsic scatter at the 1-, 2-, and 3 σ level due to fluctuations in the absorber properties (column density, Doppler parameter, redshift) along different lines-of-sight. The numerical simulations consist of Monte Carlo realizations of distributions of the absorber properties constrained from observations.

We compare our and previous measurements of the cosmic flux decrement to the outcomes of our simulations and find an excellent agreement between the observations and the predictions of one of the models considered in this work. Furthermore, we find that the distribution of the D_A values at a given redshift are well described by a lognormal distribution function. This implies that the effective optical depth, usually defined as the logarithm of the average flux, is necessarily Gaussian distributed, in contrast to previous studies. This result is independent to the form of the input distribution functions, and rather insensitive to the presence of high-column density absorbers, such as the Lyman limit systems.

Key words: methods: numerical, intergalactic medium, quasars: absorption lines

1 INTRODUCTION

Since the introduction of the Gunn-Peterson (GP) test by Gunn & Peterson (1965), a detailed knowledge about the physical state of the intergalactic medium (IGM) has been gained from the study of the absorption features identified in the spectra of quasi-stellar objects (QSOs) at restframe wavelengths $\lambda \leq 121.5$ nm, which are now known to be mainly due to resonant scattering by intergalactic neutral hydrogen, randomly distributed along the line-of-sight, as first proposed by Lynds (1971). For instance, the null result in the search for a GP trough has been used to rule out the existence of a hot intercloud medium (ICM) (Steidel 1987a, Giallongo, Cristiani & Trevese 1992, Giallongo et al. 1994), which was thought to confine by pressure the Ly α clouds (Sargent et al. 1980, Ostriker &

Ikeuchi 1983). As a result of detailed analyses of the line statistics of the absorbing material, a wealth of information on its clustering (see *e.g.* Ostriker, Bajtlik & Duncan 1988), in particular the existence of voids (*e.g.* Pierre, Shaver & Iovino 1988, Duncan, Ostriker & Bajtlik 1989, Dobrzycki 1991), and the evolution of its number densities, column densities, and Doppler parameter with redshift (*e.g.* Kim et al. 1997) has accumulated over the past years. These results, in combination with the use of state-of-the-art numerical simulations of structure formation based on the currently accepted paradigm of the concordance cosmology (Springel et al. 2005), show that the features seen in absorption against bright background sources arise when the line-of-sight intersects the structures that naturally emerge and evolve with time under the influence of gravitational attraction. Different types of structures such as the filaments present in the *cosmic web*, galactic haloes, and even the discs of primeval galaxies, give rise to distinct absorption features

* E-mail: tepper@astro.physik.uni-goettingen.de

attributed to entities known historically as Ly α Forest clouds, Lyman limit systems (LLSs), and damped Lyman absorbers (DLAs) (see *e.g.* Rauch 1998, Wolfe, Gawiser & Prochaska 2005, for excellent reviews, respectively). Nevertheless, the relation between the observed absorption features and the objects causing them, in particular the correlation between observed damped absorption lines, metal lines (*e.g.* Mg II, O VI) and galaxies—the so-called Absorber-galaxy Connection—is still a matter of debate (see *e.g.* Williams, Shu & Ménard 2005, Part 1). As a consequence of numerous efforts over many years, we now have a better understanding of the origins of the different absorption features observed in QSO spectra. In particular, the notion of discrete, intervening H I absorbing systems randomly distributed along the line-of-sight has been embedded into the more general picture of an evolving *continuous* intergalactic medium with a H I density field that varies in space and time, with its evolution driven mainly by the Hubble expansion, the radiation field of ionising UV sources, and the collapse of structures due to gravity.

1.1 Methods and Input Distributions: A Brief Review

Over decades many people have been working hard towards inferring the physical properties of the intergalactic medium such as its chemical content, density, temperature, etc. by measuring *e.g.* the type of transition, strength, number density, and profiles of absorption lines imprinted in the spectra of QSOs and Gamma-Ray bursts (GRBs) (*e.g.* Lamb & Reichart 2000). There has also been a great effort to quantify the effect of the absorption due to intergalactic neutral hydrogen on the photometric properties of background sources. As a matter of fact, several models have been developed in order to account for this so-called intergalactic attenuation, with different approaches and purposes. Møller & Jakobsen (1990) used Monte Carlo simulations to estimate the amount of absorption at wavelengths shorter than the redshifted H α λ 30.4 nm line, in order to test the feasibility of the equivalent of the Gunn-Peterson test for intergalactic helium. They found that the absorption as a function of wavelength, averaged over many lines-of-sight, should display together with a characteristic stair-case profile due to the cumulative absorption at the H I resonant wavelengths, an additional characteristic valley-shaped feature (the “Lyman-valley”) due to the cumulative effect of the photoionisation of H I by photons with energies $E_\gamma \geq hc/\lambda_L$, where $\lambda = 91.2$ nm. Later on, in a seminal paper Madau (1995) developed an analytical method to quantify the opacity due to intergalactic H I as a function of redshift, and its effect on the colors of high-redshift galaxies. The underlying assumption of this model is that the observed flux of a source at redshift z is given by the product of the *intrinsic* flux and a transmission factor that accounts for the *mean* absorption as a function of wavelength given in the form $\exp(-\tau_{\text{eff}}) \equiv \langle \exp(-\tau) \rangle$ (see equation (3) of Madau 1995), where the brackets denote the average over an ensemble of random lines-of-sight. The most common application of this model consists in correcting the flux of a synthetic spectrum for intergalactic absorption. This correction is of particular importance at high redshift, where the absorption due to intergalactic H I severely absorbs the light of a background object at restframe wavelengths shorter than 121.6 nm, leading to a substantial reddening of its colour (see *e.g.* Bicker et al. 2004). As the numerous references in the literature attest, the Madau model has become the most widely used attenuation model. However, in a later work Bershadsky, Charlton & Geoffroy (1999) argued that it is not possible to estimate the mean change in the magnitude of a source at a given redshift due to absorption by intergalactic H I along the line-of-sight by multiply-

ing the mean transmission curve of Madau’s model with the spectrum of the source and integrating over the corresponding passband, mainly because of the existence of color terms. They suggested that the correct way of accounting for the mean effect of H I absorption on the spectrum of a background source and on its photometric properties, is to model first the absorption along many random lines-of-sight, compute the desired photometric quantities for each one of them, and *then* compute the average over all lines-of-sight. In other words, they argue that the processes of averaging over many random lines-of-sight and measuring photometric quantities are non-commutative. Indeed, they showed using a Monte Carlo technique that the average magnitudes computed following their approach substantially differ from those computed using Madau’s model, even when using the same input distributions for the number of absorbers, their column densities and Doppler parameters. The approach proposed by Bershadsky et al. (1999) effectively mimics the measurement process that would take place if one would determine *e.g.* the mean observed brightness of a collection of galaxies with different absorber populations along their particular lines-of-sight, but otherwise identical in their intrinsic properties (spectrum, morphology, etc.), and is hence physically meaningful. It turns out that features such as the characteristic stair-case profile and the Lyman-valley cannot possibly be observed in a *single* spectrum, since they arise only by averaging over sufficient numbers of lines-of-sight, a process that has no physical meaning. Surprisingly, however, the Bershadsky et al. (1999) approach is rarely referenced or used in the literature.

In a more recent paper, Meiksin (2006) developed a method to compute the opacity due to intergalactic H I by using hydrodynamical simulations of structure formation in the framework of the concordance Λ CDM cosmology performed by Meiksin & White (2004). Applying his model to compute broad-band magnitudes for different types of objects (*e.g.* starburst galaxies, QSOs of Type I and II), Meiksin (2006) reports differences of 0.5 – 1.0 mag with respect to Madau (1995)’s model. Despite of the different results obtained, this model is similar to Madau (1995)’s model in the sense that it implicitly assumes that the mean opacity of the IGM along a random line-of-sight due to the presence of H I can be accounted for by multiplying a given input spectrum with a mean attenuation curve of the form $\exp(-\tau_{\text{eff}})$ and integrating over the corresponding filter function (Meiksin 2006, equation 8).

Following Bershadsky et al. (1999), we state that

$$\int_0^\infty f_\lambda \langle \exp(-\tau) \rangle T(\lambda) d\lambda \neq \left\langle \int_0^\infty f_\lambda \exp(-\tau) T(\lambda) d\lambda \right\rangle, \quad (1)$$

where f_λ is the intrinsic flux, $T(\lambda)$ is the filter transmission function, and the brackets indicate the average over all lines-of-sight. We consider that the operation denoted by the right-hand side of this expression is the correct way of estimating mean magnitudes of background objects including the effect of the absorption due to intergalactic H I. This approach is of course not restricted to the computation of mean magnitudes and colors, and can be applied to the estimate of the mean of any photometric quantity. Furthermore, it is also possible to determine not only the mean, but in principle any desired confidence interval around the mean, *e.g.* $\pm\sigma$ range, via the computation of quantiles (see Section 5).

It should be clear that not only the method, but also the input physics is an (even more) crucial ingredient of a particular model that accounts for the intergalactic attenuation, as already shown by Bershadsky et al. (1999). It is, however, not trivial to test whether using a particular method and a set of input distributions accurately describes the observed effect of the absorption by intergalactic H I

on the spectra of background sources. For example, the evolutionary synthesis models of Bicker et al. (2004) that include the correction for intergalactic absorption based on Madau's model match quite well the observations of galaxies in the Hubble Deep Field (see his Figure 12), since the magnitude differences reported by (Bershady et al. 1999, Figure 7) with respect to the latter model are in this case of the order of the scatter of the observations around the predicted colors. In other words, even though these models are fundamentally different, it is difficult to test the accuracy of their predictions on the basis of a comparison to *e.g.* observed galaxy colors. A quantity that is more sensitive to the absorption due to intergalactic H I is the mean cosmic flux decrement D_A (cf. Section 2). The reason for this is that the restframe wavelength range over which this quantity is measured is typically 10 nm wide, and is hence narrower than typical broadband filters. We thus consider as a primer test that any model that accounts for the absorption due to intergalactic H I should reproduce first of all the observations of this quantity. On this basis, it should be possible to discriminate between models through the comparison of their respective predictions to measurements of D_A . As we will show, the input distributions used by Bershady et al. (1999) to estimate changes in the magnitude of background galaxies do not match the observations of D_A very well, and thus the results of that model regarding galaxy colors should be taken with caution. We will show that Madau's model and Bershady et al. (1999)'s model are complementary to each other in the sense that the input physics of the first, with the approach of the second, truly match the measurements of the cosmic flux decrement.

To sum up: The main goal of this work is to compute and analyse the evolution of D_A with redshift for different evolution scenarios of the intergalactic neutral hydrogen, conveniently parametrized by input distribution functions of the form of equation (4, cf. Section 2). Thus, the models we present here differ only by the set of input distribution functions used, but they all equal in method, *i.e.* all of them take advantage of the Monte Carlo technique. We judge the goodness of a particular model by its power to reproduce the observations of D_A in a wide redshift range. Once we identify such a model, we exploit it to analyse some interesting properties of D_A . In a forthcoming paper, we will make use of such a model to assess the impact of the stochastic absorption due to intergalactic H I on the photometric properties of high-redshift galaxies.

This work is organised as follows: In Section 2 we briefly recall the concept of the cosmic flux decrement and discuss some issues related to its measurement. In Section 3 we present two different types of models for the intergalactic attenuation, which we use to compute the redshift evolution of the cosmic flux decrement. In Section 4, we describe our measurements of this quantity for a sample of SDSS QSO spectra. Finally, we compare these and previous measurements to the outcomes of each model, and discuss the results of this comparison as well as some other implications of the models for the evolution of D_A in Section 5.

2 THE COSMIC FLUX DECREMENT REVISITED

Before high-resolution (*i.e.* $\Delta\lambda \lesssim 1$ nm), high S/N observation became feasible, the basic spectroscopic technique used to analyse the effect of the absorption due to intergalactic neutral hydrogen on the spectra of background sources was to measure the mean depression of the observed flux relative to the unabsorbed flux—also called

continuum—, a quantity which became to be known as cosmic flux decrement. This quantity, first introduced by Oke & Korycansky (1982), can be defined as a function of redshift by

$$D_A(z) \equiv \frac{1}{\Delta\lambda} \int_{\lambda_1(1+z)}^{\lambda_2(1+z)} \left(1 - \frac{f_{obs}(\lambda)}{f_c(\lambda)} \right) d\lambda, \quad (2)$$

where f_c and f_{obs} are the continuum and the observed fluxes, respectively, and $\Delta\lambda \equiv (1+z) \cdot (\lambda_2 - \lambda_1)$. Formally, the integral is computed in the restframe wavelength range [102.5, 121.6] nm, *i.e.* between the Ly α and the Ly β emission lines. However, the actual estimate of D_A is usually performed between the restframe wavelengths 105 nm and 117 nm—or in an even narrower wavelength interval—in order to avoid contamination by the emission wings of the Ly β + OVI and Ly α lines, respectively.

The cosmic flux decrement effectively measures the *total* equivalent width of all Ly α absorption lines in the chosen wavelength range, if corrected for the contribution of metal absorption lines. This idea has indeed been used by Zuo & Lu (1993) in order to measure this quantity by adding up the equivalent widths of lines identified as Ly α absorption lines in a given wavelength range, thus avoiding the contamination from metal lines. Of course, the reliability of this measurement highly depends on the correct identification of lines, a task that is not trivial at all.

Since D_A is extremely sensitive to f_c , as can be easily seen from the definition (2), an accurate measurement of this quantity demands a reliable estimate of the underlying continuum. Unfortunately, there is no consensus of what the best method to estimate the continuum may be. A popular choice, mainly because of the presence of emission lines in the Ly α forest region, consists in fitting a local continuum, most commonly using cubic splines (see *e.g.* Lu et al. 1996) or b-spline functions (see *e.g.* Kirkman et al. 2003, Tytler et al. 2004a,b), searching for regions apparently free of absorption blueward of the Ly α emission line. Other authors prefer to fit a continuum in the region redward of the red wing of the Ly α emission line, and extrapolate it to the region blueward of it (Steidel & Sargent 1987b, Schneider et al. 1989, Cristiani et al. 1993). A widely adopted form for the fitted continuum in this case is a power-law with spectral index α_ν with measured values in the range [0.28, 0.99] (Steidel 1987b, Vanden Berk et al. 2001, and references therein). The latter method usually tends to place the intrinsic continuum level higher than it actually is, thus overestimating the measured values of D_A ; for the former method the opposite is true, in general. For either method, there is an uncertainty in the estimate of the continuum, and this is the main drawback of the mean flux depression as a technique to estimate the mean absorption due to neutral hydrogen present in the intergalactic medium (IGM). However, it turns out that reliable measurements of D_A are very useful to constrain estimates of fundamental cosmological parameters such as the mean baryon density Ω_b , the UV background intensity (see *e.g.* Rauch et al. 1997), the normalization of the power spectrum σ_8 , the vacuum-energy density Ω_Λ , and the Hubble parameter H_0 (Tytler et al. 2004a).

The evolution of the cosmic flux decrement has been previously modeled by different workers (see *e.g.* Giallongo, Gratton & Trevese 1990, Cristiani et al. 1993, Madau 1995), usually obtaining a good agreement with observations. However, there is still a scatter in the observations of this quantity for which it has not been accounted yet in any modelling so far. Using our Monte Carlo simulations of the absorption due to intergalactic H I along a large number of lines-of-sight, we assess to which extent the observed scatter can be ascribed to the *intrinsic* scatter in D_A due to fluctuations in

the absorber properties (number density, column density, Doppler parameter) along different lines-of-sight (see Section 5.3).

Under the assumption that the restframe equivalent width of the absorbers does not evolve with redshift, and that the number density of the absorbing systems evolves like $\propto (1+z)^\gamma$, It is expected that D_A should evolve with z like

$$D_A(z) \propto (1+z)^{1+\gamma} \quad (3)$$

where the factor $(1+z)$ comes from the scaling of the equivalent width, as pointed out by Jenkins & Ostriker (1991). Indeed, it has been found empirically that the redshift evolution of D_A can be described by a power law $D_A(z) = A \cdot (1+z)^\gamma$ with $A = 6.2 \cdot 10^{-3}$ and $\gamma = 2.75$ (Kirkman et al. 2005), but also by an exponential $D_A(z) = D_A^0 \cdot e^{\alpha(1+z)}$ with $D_A^0 = 0.01$ and $\alpha = 0.75$ (Zhang et al. 1997). More recently, Kirkman et al. (2007) showed that the observed evolution of D_A with redshift in the range $0 < z < 3.2$ is well described by a broken power-law, even though the fit is still poor. None the less, expression like these are only valid up to a given redshift, since it diverges for $z \rightarrow \infty$, whilst D_A converges asymptotically to 1 in this limit, or more precisely, when z approaches the redshift z_{reion} at which reionisation sets on. Furthermore, even if the power-law form for the evolution of D_A holds, the index γ in the last equation should be replaced by $\bar{\gamma}$, where the latter index accounts for the averaged evolution of absorbers of different column densities. As we know now, different types of absorbers evolve at different rates, and an equation of the form (3) would imply that they evolve at the same rate, independently of their column density. On the other hand, estimates of a single γ from D_A measurements assuming a power-law of the form of equation (3), as done by O'Brien, Wilson & Gondhalekar (1988), may give a hint on the population of absorbers *dominating* the behaviour of D_A , comparing the estimated γ with the power-law index of the different populations. We will show from our simulations that the predicted redshift evolution of D_A satisfies the asymptotic behaviour described above, and that, indeed, this behaviour is dominated by the absorbers with column densities $N_{HI} \lesssim 10^{17} \text{ cm}^{-2}$.

A compilation of D_A measurements, accumulated in the literature over the past twenty years approximately, and which includes our own measurements that extend the redshift range to $z_{em} = 5.41$, is shown in Figure 2 (cf. Section 4 and cited references for details on the measurements in this figure).

3 MODELLING THE INTERGALACTIC ATTENUATION

Since the observation of individual sources (galaxies, QSOs, GRBs) necessarily implies observations along different lines-of-sight, it is expected that the stochastic nature of the distribution of the Ly α absorbers, especially of those with the highest column densities, causes a scatter in the observed absorption, even for sources with identical intrinsic spectra. Hence, depending on the absorption along a particular line-of-sight, one would expect different observed values for each measurement of any photometric quantity, for example, the cosmic flux decrement D_A . Performing enough measurements of such a quantity for nearly "identical" sources at a fixed redshift, one could in principle estimate its mean and its scatter due to stochastic effects in the absorption by neutral hydrogen in the IGM.

The numerical realisation of this thought experiment is best achieved through Monte Carlo simulations. Following *e.g.* Møller

Table 1. Types of absorbers and their corresponding parameters adopted from Madau (1995, equation 10). Note, however, that he quotes as lowest column density $N_{HI} = 2.0 \cdot 10^{12}$, while we use $N_{HI} = 1.0 \cdot 10^{12}$, in order for the adopted normalisation to be consistent.

$N_{HI} [\text{cm}^{-2}]$	\mathcal{N}_0	γ	β
$10^{12} - 1.59 \cdot 10^{17}$	$2.40 \cdot 10^7$	2.46	1.50
$1.59 \cdot 10^{17} - 10^{20}$	$1.90 \cdot 10^8$	0.68	1.50

Table 2. Types of absorbers and their corresponding parameters. Parameters are adopted from Bershadsky, Charlton & Geoffroy (1999, equation 10).

$N_{HI} [\text{cm}^{-2}]$	\mathcal{N}_0	γ	β
$10^{12} - 10^{14}$	$3.14 \cdot 10^7$	1.29	1.46
$10^{14} - 1.59 \cdot 10^{17}$	$1.70 \cdot 10^6$	3.10	1.46
$1.59 \cdot 10^{17} - 10^{20}$	$1.90 \cdot 10^8$	0.68	1.50

& Jakobsen (1990), Giallongo et al. (1990), Cristiani et al. (1993), Bershadsky et al. (1999), we generate thousands ($4 \cdot 10^3$) of lines-of-sight each with a random population of H I absorbers, and compute the absorption along each of them for a given input spectrum at a fixed redshift. The population of each line-of-sight consists of a random number N_{abs} of absorbing systems, each of them characterized by three parameters: its redshift z_{abs} , its column density N_{HI} , and its Doppler parameter $b \equiv \sqrt{2kT/m_H}$, where k is the Boltzmann constant, T is the kinetic temperature of the gas and m_H is the mass of the hydrogen atom.

The redshift and column density characterising each absorber are drawn from a distribution of the form

$$f(N_{HI}, z) = \mathcal{N}_0 \cdot (1+z)^\gamma \cdot N_{HI}^{-\beta}, \quad (4)$$

where \mathcal{N}_0 is a normalization constant. This function defines the 1-dimensional distribution of the H I present in the IGM probed by a random line-of-sight. The number N_{abs} of systems for each line-of-sight is drawn from a Poisson distribution with parameter

$$\langle N_{abs} \rangle = \int_{I_z} \int_{I_{N_{HI}}} f(N_{HI}, z) dN_{HI} dz, \quad (5)$$

where the integral is carried out over appropriate redshift- and column density intervals I_z and $I_{N_{HI}}$, respectively.

We use different sets of input distributions that include the evolution of both low- and high density absorbers, and that give rise to the following models:

MMC This model relies on the input distributions from Madau (1995, equation 10) listed in Table 1. Here, the Doppler parameter is kept constant at a value $b = 35.0 \text{ km s}^{-1}$, which corresponds approximately to the mean derived by Rauch et al. (1992).

BMC This model matches the model named MC-Kim of Bershadsky et al. (1999), but we briefly describe it here for completeness. The corresponding parameters for the line-density evolution and column density distribution functions are summarized in Table 2. In this model, in contrast to the MMC model, the Doppler parameter for each absorber is drawn from a truncated, redshift-dependent Gaussian distribution of the form

$$P(b) \equiv \Theta(b - b_{tr}) \cdot \frac{1}{\sqrt{2\pi\sigma^2}} \exp\left(-\frac{1}{2\sigma^2}(b - \mu)^2\right),$$

where $\Theta(x)$ is the Heaviside function:

$$\Theta(x) = \begin{cases} 0, & x < 0 \\ 1, & x \geq 0 \end{cases}$$

and the mean, standard deviation and truncation value at redshift z are given by $\mu(z) = -3.85z + 38.9$, $\sigma(z) = -3.85z + 20.9$ and $b_{tr}(z) = -6.73z + 39.5$, respectively. Bershadsky et al. (1999) originally used this model to analyse the impact of the intergalactic attenuation in the range $1.75 < z < 5.0$, but we use it in the extended range $0.2 < z < 5.41$. Since our highest redshift limit is not too far away from Bershadsky et al.'s, we consider the model to be valid in our extended redshift range.

MMC without Lyman limit systems In order to assess the impact of the Lyman limit systems on the intergalactic absorption, we introduce this model, which consists of the same input distributions as the MMC model, excluding the systems with column densities $N_{\text{HI}} > 1.59 \cdot 10^{17} \text{ cm}^{-2}$.

In all the models describe above, the attenuation factor for each absorber is given by $\exp[-\tau(\lambda)]$, where, for the general case, the absorption coefficient $\tau(\lambda)$ can be written as

$$\tau(\lambda) = \tau_{LL}(\lambda) + \sum_{i=2}^{N_{\text{trans}}} \tau_i(\lambda). \quad (6)$$

The first term on the right-hand side is the opacity due to the ionisation of neutral hydrogen by photons with wavelengths $\lambda \leq \lambda_{LL} \equiv 91.18 \text{ nm}$. It is given by

$$\tau_{LL}(\lambda) = N_{\text{HI}} \cdot g(\lambda) \cdot \sigma_{\infty} \cdot \left(\frac{\lambda}{\lambda_{LL}}\right)^3, \quad (7)$$

where $\sigma_{\infty} \equiv 6.3 \cdot 10^{-18} \text{ cm}^2$ is the H I photoionisation cross-section, and g is the Gaunt-factor for bound-free transitions¹. The second term is the sum of the opacities due to resonant scattering at each transition of the Lyman series². In general, the absorption coefficient for the transition $n = i \rightarrow 1$ is

$$\tau_i(\lambda) = N_{\text{HI}} \cdot \sigma_i \cdot \phi(a_i, x). \quad (8)$$

The cross-section σ_i is a function of the Doppler parameter b , the oscillator strength of the transition f_i , and the resonant wavelength λ_i , and is given by

$$\sigma_i = \frac{\sqrt{\pi} e^2}{m_e c^2} \frac{\lambda_i^2}{\Delta\lambda_D} f_i, \quad (9)$$

where $\Delta\lambda_D = \lambda_i b/c$ is the Doppler broadening, and the variable $x \equiv (\lambda - \lambda_i)/\Delta\lambda_D$ is the distance to the line center in Doppler units. We assume the profile function ϕ of the absorption line to be given by the Voigt-Hjerting function

$$H(a_i, x) \equiv \frac{a_i}{\pi} \int_{-\infty}^{+\infty} \frac{e^{-y^2}}{(x-y)^2 + a_i^2} dy. \quad (10)$$

¹ An extensive tabulation of values for the Gaunt-factor can be found in Karzas (1961).

² We adopt the convention that the Ly α transition (from the ground state to the next higher energy level) be identified with $i = 2$, the Ly β transition with $i = 3$, etc. The photoionisation cross-section is thus consistently denoted by σ_{∞} .

Here, $a_i \equiv \lambda_i^2 \Gamma_i / (4\pi \Delta\lambda_D)$ is the relative strength of the natural broadening to Doppler broadening for the i th transition, and $y \equiv v/b$ is the kinetic velocity in units of the Doppler parameter. In this work, we neglect the opacity due to the photoionisation term and consider only the first resonant transition, *i.e.* the Ly α transition, since this is the only one of interest in the wavelength range studied here. Furthermore, we use the approximation to H for values of a and column densities characteristic for intergalactic H I of Tepper García (2006).

3.1 The transmission factor Φ

The cumulative absorption along a random line-of-sight of the flux f_{em} of a source at redshift z_{em} is calculated according to expression

$$f_{obs}(\lambda_{obs}) = \frac{f_{em}(\lambda_{em})}{1 + z_{em}} \cdot \Phi(\lambda_{abs}), \quad (11)$$

where λ_{obs} , λ_{em} and λ_{abs} are the observed wavelength, the emitted wavelength, and the wavelength at absorption, respectively. These are related by $\lambda_{obs} = \lambda_{abs} \cdot (1 + z_{abs}) = \lambda_{em} \cdot (1 + z_{em})$. The quantity Φ is the transmission factor and is given by

$$\Phi(\lambda) \equiv \prod_{i=1}^{N_{abs}} \exp[-\tau_2(\lambda/(1+z_i))] = \exp\left[-\sum_{i=1}^{N_{abs}} \tau_2(\lambda/(1+z_i))\right], \quad (12)$$

where τ is given by equation (8), and z_i is the redshift at the epoch of absorption³.

Introducing the relation $f_c(\lambda) = f_{em}[\lambda/(1+z)]/(1+z)$, it follows from equations (2) and (12) that

$$1 - D_A(z) = \frac{1}{\Delta\lambda} \int_{\lambda_1(1+z)}^{\lambda_2(1+z)} \Phi(\lambda) d\lambda. \quad (13)$$

Note that the right-hand side of this expression is just wavelength-averaged value of Φ at redshift z , and we will denote it by $\bar{\Phi}_z$. Note, however, that this quantity still depends on redshift, as indicated by the subscript. Since $D_A(z)$ and $\bar{\Phi}_z$ differ only by a constant factor, they may be considered as equivalent with respect to their statistics, which will be discussed in Section 5.2.

4 OUR D_A MEASUREMENTS

We want to compare the predictions for the evolution of D_A that result from the models described above to observations. For this purpose, we use previous measurements of D_A reported in the literature, and we perform ourselves new measurements of this quantity, extending the redshift range of the measurements to $z_{em} = 5.41$. Our own measurements are done on QSO spectra from the SDSS Data Release 5.

Our selection procedure of sources suitable for this purpose was as follows: since the wavelength range available from SDSS (DR5) is $\lambda \in [380, 920] \text{ nm}$, and we measure the continuum depression D_A in the restframe wavelength interval $\lambda \in [105, 117] \text{ nm}$, the redshift of our sample is restricted to $z_{min} \geq 380/105 - 1 = 2.62$. We choose $z_{min} = 2.7$ as our lowest redshift in order to avoid the low S/N at the blue end of the spectrograph. A simple query for high- z quasi-stellar objects on the SDSS SkyServer Spectroscopic

³ The reader shall bear in mind that N_{HI} , and σ_i and a_i —through the dependence on the Doppler parameter—in equation (8) are different in general for each absorber. However, we do not write this explicitly by *e.g.* introducing a new subscript in order to avoid a cumbersome notation.

Query Form with this only restriction returns around 2400 spectra. From this first selection, we rejected those objects for which the redshift was either not measured, the measurement had failed, or the measured photometric and spectroscopic redshifts were inconsistent with each other. We then binned the quasars in redshift intervals of $\Delta z = 0.1$ and selected for each redshift bin the spectrum with the highest S/N, leaving us with 28 sources, from which we removed three further objects due to low data quality. The resulting sample is listed in Table 3.

4.1 Continuum fit

The continuum of a quasi-stellar source is often assumed to be of the form $f_\nu = f_\nu^0 \nu^{-\alpha_\nu}$ (see *e.g.* Steidel 1987b, Laor et al. 1997, Zheng et al. 1997), or equivalently, $f_\lambda = f_\lambda^0 \lambda^{-\alpha_\lambda}$, where both indices are related by $\alpha_\lambda = 2 - \alpha_\nu$, and $f_\lambda^0 = f_\nu^0 \cdot c^{1-\alpha_\nu}$, and c is the speed of light. Despite of the fact that the spectral index α_λ varies over large wavelength ranges (see *e.g.* Neugebauer et al. 1979), Zheng et al. (1997) find by constructing a composite QSO spectrum from 284 HST FOS spectra, that a single power-law describes well the continuum for wavelengths between 105 and 220 nm, but that the continuum steepens significantly for $\lambda \leq 105$ nm. Analogously, constructing a composite QSO spectrum from a homogeneous sample of over 2200 SDSS QSOs, Vanden Berk et al. (2001) find that the continuum in the rest-frame wavelength range $\lambda < 500$ nm can be very well modeled by a single power-law either in wavelength or frequency. However, as already mentioned in Section 2, other authors prefer to fit continua locally using cubic splines (see *e.g.* Lu et al. 1996) or b-spline functions (see *e.g.* Kirkman et al. 2003, Tytler et al. 2004a,b) searching for regions apparently free of absorption blueward of the Ly α emission line.

Since the Ly α forest region is severely absorbed due to intervening H I systems, especially for high- z QSOs, and a local fit to the continuum in this region is extremely difficult, we choose to estimate the continuum of our selected sources in the Ly α forest region by fitting a power-law to the QSO spectrum redward of the Ly α emission line and extrapolating it for $\lambda \leq 121.567$ nm in the restframe of the source. As long as the assumption of the underlying power-law holds, this approach has the advantage that the continuum estimate is completely independent of the spectral resolution and S/N in the Ly α forest region. It is true, however, that due to the steepening blueward of $\lambda = 105$ nm found by Zheng et al. (1997), fitting the continuum of each source redward of Ly α with a single power law and extrapolating it to shorter wavelengths may tend to underestimate the absorption in the Ly α forest region. Nevertheless, and due to a fortunate coincidence, the measurements of D_A are usually performed precisely for $\lambda \geq 105$ nm to avoid the wings of the Ly β + OVI emission lines. Thus, the assumption of an underlying continuum in the form of a *single* power-law, and consequently the measurements of D_A assuming such a continuum, are more than validated in the light the results mentioned above.

The power-law that we fit to each spectrum is of the form

$$f_c(\lambda; \alpha_\lambda) = f_\lambda^0 (\lambda + \lambda_0)^{\alpha_\lambda}. \quad (14)$$

where the flux amplitude f_λ^0 , the wavelength off-set λ_0 , and the spectral index α_λ are the parameters to be determined. We fit the continuum in the wavelength range $[130 \cdot (1 + z_{em}), 900]$ nm, in order to avoid the red emission wing of the Ly α line and the red end of the spectrograph, respectively. Note, however, that for redshifts $z_{em} \gtrsim 5$ the available wavelength range is smaller than 120 nm, and this may introduce a large uncertainty in the fitted continuum. The fit parameters and their uncertainties were obtained with help

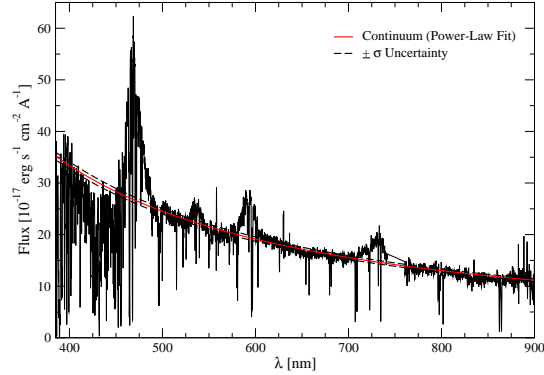


Figure 1. Spectrum of the QSO SDSS J112107.99+513005.4 at $z_{em} = 2.843$. The heavy solid and heavy dashed line indicate the power-law fit to the continuum and its uncertainty, respectively. The corresponding spectral index is $\alpha_\lambda = 1.256 \pm 0.003$.

of the IDL task CURVEFIT. It turns out that the continuum fit is rather insensitive to the uncertainties in the flux amplitude and the wavelength off-set, and extremely sensitive to the uncertainty in the spectral index. Because of this and for simplicity, in our further analysis we neglect the error in the first two parameters and consider only the uncertainty in the spectral index to be of relevance⁴. The spectral index and its uncertainty for each source is listed in Table 3. An example of a QSO spectrum and its corresponding fit are shown in Figure 1.

4.2 Measurement of D_A

For each QSO spectrum, we compute the *total* absorption pixel by pixel in the range $\lambda \in [105, 117]$ nm according to the expression

$$D_A(z_{em}; \alpha_\lambda) \equiv \frac{1}{N_{pix}} \sum_{i=1}^{N_{pix}} \left(1 - \frac{f_{obs}(\lambda_i)}{f_c(\lambda_i; \alpha_\lambda)} \right), \quad (15)$$

where N_{pix} is the total number of pixels between $\lambda_1 = 105 \cdot (1 + z_{em})$ nm, $\lambda_2 = 117 \cdot (1 + z_{em})$ nm. As a consistency check, we adopt two different methods to estimate the error in our measurements of D_A . The first method assumes that the $\pm\sigma$ range for each measurement is given by $D_A[z_{em}; \alpha_\lambda \pm \sigma(\alpha_\lambda)] - D_A[z_{em}; \alpha_\lambda]$, respectively, for the corresponding values of $\sigma(\alpha_\lambda)$ listed in Table 3. The second method is based on error propagation, according to which the error $\sigma(f)$ in the estimate of a quantity $f(x_i)$, which depends on n independent random variables $\{x_i\}$, each with an uncertainty $\sigma(x_i)$, is given by

$$\sigma^2(f) = \sum_{i=1}^n \sigma^2(x_i) \cdot \left(\frac{\partial f}{\partial x_i} \right)^2. \quad (16)$$

In the case of our measurements of D_A , only the uncertainty in the index α_λ is relevant, and hence equation (16) becomes

⁴ The full list of fit parameters for each source and their uncertainty will be available in machine-readable form at <http://astro.physik.uni-goettingen.de/~tepper/da/fitparam.txt>

Table 3. QSO sample selected from the SDSS DR5. The first four columns include the object designation^a, the emission redshift as quoted in the SDSS DR5 catalog, the spectral index used for fitting the continuum, and its uncertainty, respectively. The last two columns give the measurement of D_A and its uncertainty, together with additional error estimate (see text for details.)

Object	z_{em}	α_λ	$\sigma(\alpha_\lambda)$	D_A	$\sigma_{err}(D_A)$
SDSS J115538.60+053050.5	2.712	-1.213	0.002	$0.390^{+0.010}_{-0.010}$	0.010
SDSS J112107.99+513005.4	2.843	-1.256	0.003	$0.281^{+0.015}_{-0.016}$	0.015
SDSS J010619.24+004823.3	2.882	-1.170	0.003	$0.294^{+0.018}_{-0.018}$	0.018
SDSS J075618.13+410408.5	2.956	-1.320	0.007	$0.329^{+0.038}_{-0.040}$	0.039
SDSS J164219.89+445124.0	3.125	-1.550	0.001	$0.349^{+0.005}_{-0.005}$	0.005
SDSS J004054.65-091526.8	3.185	-1.278	0.000	$0.459^{+0.000}_{-0.000}$	0.000
SDSS J124306.55+530522.1	3.317	-1.255	0.012	$0.426^{+0.057}_{-0.064}$	0.060
SDSS J083122.57+404623.4	3.365	-1.230	0.003	$0.261^{+0.017}_{-0.017}$	0.017
SDSS J085343.32+370402.3	3.475	-1.115	0.005	$0.527^{+0.019}_{-0.020}$	0.020
SDSS J093523.32+411518.7	3.566	-1.407	0.007	$0.396^{+0.036}_{-0.039}$	0.038
SDSS J094349.65+095400.9	3.713	-1.199	0.014	$0.529^{+0.057}_{-0.064}$	0.060
SDSS J023137.64-072854.5	3.750	-1.269	0.008	$0.462^{+0.037}_{-0.039}$	0.038
SDSS J144717.97+040112.4	3.931	-1.303	0.016	$0.525^{+0.062}_{-0.072}$	0.067
SDSS J162331.15+481842.1	3.990	-1.113	0.006	$0.494^{+0.022}_{-0.023}$	0.023
SDSS J014049.18-083942.5	4.112	-1.181	0.010	$0.488^{+0.041}_{-0.044}$	0.042
SDSS J234150.01+144905.9	4.155	-1.094	0.010	$0.558^{+0.035}_{-0.038}$	0.036
SDSS J081240.68+320808.6	4.332	-1.074	0.028	$0.517^{+0.100}_{-0.127}$	0.113
SDSS J103601.03+500831.8	4.449	-1.149	0.012	$0.612^{+0.039}_{-0.043}$	0.041
SDSS J162626.50+275132.4	4.580	-1.187	0.023	$0.681^{+0.057}_{-0.069}$	0.062
SDSS J005006.35+005319.2	4.663	-1.204	0.018	$0.693^{+0.043}_{-0.049}$	0.046
SDSS J083914.14+485125.7	4.885	-1.350	0.030	$0.737^{+0.057}_{-0.073}$	0.064
SDSS J163950.52+434003.7	4.976	-1.321	0.024	$0.694^{+0.056}_{-0.069}$	0.062
SDSS J233446.40-090812.3	5.107	-1.332	0.000	$0.735^{+0.000}_{-0.000}$	0.000
SDSS J101447.18+430030.1	5.275	-1.220	0.029	$0.758^{+0.058}_{-0.076}$	0.066
SDSS J142123.98+463317.8	5.414	-1.321	0.080	$0.825^{+0.087}_{-0.173}$	0.121

^a The designation of each object meets the IAU nomenclature, as required. For details on the official SDSS designation of an object, please consult www.sdss.org/dr5/coverage/IAU.html

$$\sigma_{err}(D_A) \equiv \sigma(\alpha_\lambda) \cdot \frac{1}{\Delta\lambda} \int_{\lambda_1}^{\lambda_2} \ln(\lambda + \lambda_0) \frac{f_{obs}(\lambda)}{f_c(\lambda; \alpha_\lambda)} d\lambda, \quad (17)$$

where we have used equations (14) and (15). Our D_A measurements together with the errors computed according to both methods are listed in Table 3. Note that the errors computed using equation (17) approximately (in some cases exactly) correspond to the arithmetic mean of the $\pm\sigma$ uncertainty quoted in the measurements of D_A , which were computed according to the first method.

Since we do not aim at a high-precision measurement of D_A (as done for example by Tytler et al. 2004a), we consider our error estimate satisfactory for our purposes. Because of this same reason, we do not correct our measurements for contamination of metal lines. However, this should not introduce a large error, since their contribution is small. For example, Tytler et al. (2004a) find that they contribute by 2.3 ± 0.5 per cent to the total absorption at $z =$

1.9. The validity of this assumption will be also shown in the next section by the comparison of D_A -measurements to the results of our simulations, in which the absorption due to metal lines is not included.

5 RESULTS & DISCUSSION

5.1 Observations vs. Models

We compute the evolution of D_A in the redshift interval $0.35 < z_{em} < 6.0$ using three different models to account for the intergalactic absorption: the models MMC (with and without Lyman limit systems) and BMC presented in the Section 3, which include the effect of different populations of absorbers, *i.e.* Ly α forest clouds and Lyman limit absorbers. For completeness, we include the val-

ues of D_A computed using Meiksin (2006)’s model (see Section 1). We refer to this model as MTC. For the MMC (with and without LLS) and BMC models, we simulate an ensemble of lines-of-sight at fixed redshift, and compute for each of them the flux decrement D_A according to equation (13). In this way we get for each given redshift an ensemble of D_A values for each model, from which we estimate the 50 per cent quantile (median), and the ± 34.13 , ± 43.32 , ± 47.72 , ± 49.38 , and ± 49.87 per cent quantiles around the median, which correspond to the ± 1 , ± 1.5 , ± 2 , ± 2.5 and $\pm 3\sigma$ ranges. We do not compute the mean and σ ranges in the usual way, since the distribution of D_A is unknown a priori. However, as will be shown in Section 3, the distribution of D_A is close to a lognormal or even a Gaussian distribution; thus, the identification of mean with median, of $\pm\sigma$ range with the ± 34.13 quantile around the median, and so on, is justified. Since the MTC model does not use empirical input distributions of the form of equation (4), it is not possible to apply the Monte Carlo technique to this model, and hence we do not further analyse its implications for the evolution of D_A . We compute for this model a single value for D_A for each redshift by numerically integrating the transmission function for the corresponding redshift in the restframe wavelength range [105, 117] nm.

We compare our simulations to measurements of D_A accumulated in the literature over the past two decades, done with different methods and approaches. This compilation is by no means intended to be complete. The reason for choosing these measurements is mainly that they were performed in redshift ranges which are more or less mutually exclusive, and which all together cover the range $0 < z_{em} < 4$. Thus, these previous measurements together with our own cover a wide redshift range that makes the comparison to models more rigorous. Besides, by using measurements carried on using different methods, we diminish in some way the bias introduced in the D_A measurements due to the particular method chosen by each group. This makes the comparison of observation to models even more objective. The literature data and our own measurements that extend the redshift range of the observations to $z_{em} = 5.41$, is shown together with our model calculations in Figure 2 (see cited references for details of the measurements shown).

As can be seen in Figure 2, the predictions for the evolution of D_A from all three models, MMC, BMC, and MTC, are practically indistinguishable from each other when compared to observations at $z_{em} \lesssim 3$. We do not include in this figure the predictions for D_A based on the MMC model without LLSs, since the difference between this and the full MMC model is negligible. At higher redshifts, the values of D_A obtained from the MMC and MTC models match the observations pretty well. Yet, it is not possible to discriminate between these models due to the uncertainty and the strong scatter in the observations, especially around $z_{em} \approx 3.5$ (cf. Section 5.3). In contrast to the MMC and the MTC models, the predictions from the BMC model dramatically deviate from the measurements of D_A at $z_{em} > 3$. Since the models differ only in terms of the input distributions and not in terms of the method, it is clear that the input distributions of the BMC model are not quite accurate. Furthermore, and because of the fact that the effect of attenuation is largest at large redshifts, we conclude that the magnitude changes for high- z colors reported by Bershadsky et al. (1999) are possibly erroneous, since the measurements of D_A cannot be recovered when computing its redshift evolution using their model.

We include in Figure 2 the empirical fits of Zhang et al. (1997) of the form $D_A(z) = D_A^0 e^{\alpha(1+z)}$ with $D_A^0 = 0.01$ and $\alpha = 0.75$

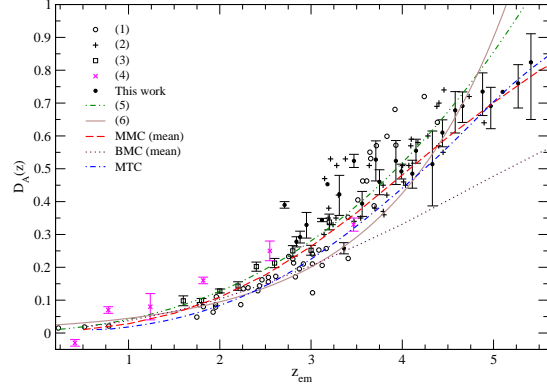


Figure 2. Evolution of D_A computed using the MMC (dashed line), BMC (dotted line), and MTC (dot-dashed line) models, compared to observations performed over the past twenty years by different groups and different methods: (1) Zuo (1993), (2) Schneider, Schmidt & Gunn (1991), (3) Kirkman et al. (2005), (4) O’Brien, Wilson & Gondhalekar (1988). Note that, despite of the heterogeneity of the approaches to measure D_A , its evolution as computed using the MMC and MTC models very accurately matches the observations, while they disagree strongly with the BMC model, especially at redshifts $z_{em} > 3.0$. Below this redshift, the models are practically indistinguishable from each other. For completeness, we include the empirical fits to the evolution of D_A from: (5) Zhang et al. (1997), and (6) Kirkman et al. (2005).

and of Kirkman et al. (2005) of the form $D_A(z) = A(1+z)^\gamma$ with $A = 0.0062$ and $\gamma = 2.75$. These empirical fits match the observations quite well at $z_{em} \lesssim 4.5$. However, as stated before, they should be taken with caution, especially at high redshifts. While D_A asymptotically converges to unity as the redshift approaches the epoch of reionisation, z_{reion} , these empirical fits do not. In contrast, the predicted evolution of D_A from all models describe above does satisfy the expected and observed asymptotic behaviour. However, the rate of convergence to this limiting value depends on the particular set of input distributions used: the stronger the number density evolution, the faster the convergence. In other words, different input distribution functions imply different values for z_{reion} , and this information may be used as a further constraint on the accuracy of a particular set of input distributions. Extending the computations of the evolution of D_A with the MMC and MTC models to redshifts $z_{em} > 6.0$, it turns out that D_A is almost unity at $z_{em} \approx 7.0$. This value is slightly higher than the value of 6.5 quoted by Fan et al. (2002) for the epoch of reionisation.

In Figure 3, we show the redshift evolution of D_A as computed from the MMC model. We show the 50 per cent quantile, i.e. the median, and the ± 34.13 , and ± 49.87 per cent quantiles, which correspond to the ± 1 -, and $\pm 3\sigma$ ranges around the median. Again, the difference between the predictions of the MMC with and without LLSs is negligible, and thus we show only the results for the full MMC model. Also shown in this figure are our measurements of D_A together with the measurements of O’Brien, Wilson & Gondhalekar (1988) from Figure 3, and the most recent measurements of D_A available in the literature from Kirkman et al. (2007). We include only these measurements, since they are the only ones that include their uncertainty, and also because these data sets fully cover the redshift range $0.2 < z_{em} < 5.41$. As can be

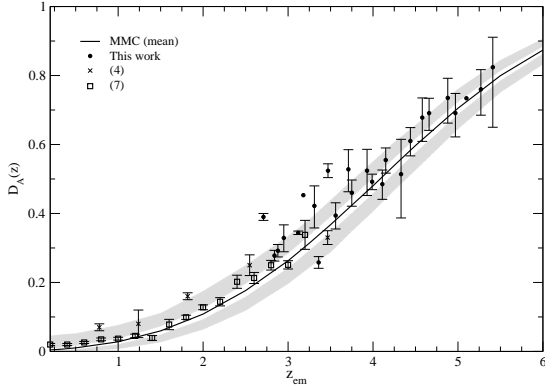


Figure 3. Evolution of the mean D_A according to the MMC model (solid line) in the range $0.2z_{em} < 6$. Here we show again our measurements of D_A , together with the most recent measurements from Kirkman et al. (2007) (7). The white and shaded areas around the solid line indicate the intrinsic scatter at the ± 1 and $\pm 3\sigma$ level, respectively, due to variation in the absorption from one random line-of-sight to another.

seen, within the uncertainty the observations are well matched by the evolution of D_A predicted by the MMC model in the redshift range $0.2 < z_{em} < 5.41$, with the exception of some outliers around $z_{em} \approx 3$, where the scatter of the observations is large, as also seen in Figure 2. As is apparent from Figures 2 and 3, the largest scatter in the observed values of D_A at a given redshift cannot be ascribed to the *intrinsic* scatter in the absorption due to variations from one line-of-sight to another, not even at the $\pm 3\sigma$ level. It may be possible that this scatter is not real, but only an artifact of the method employed to measure D_A . However, if real, this scatter indicates that the models can only reproduce well the redshift evolution of the mean D_A , but cannot account for its variation among different lines-of-sight.

None the less, since the MMC reproduces the observations within their corresponding uncertainty very well, we consider it as a fiducial model for the intergalactic absorption and explore in detail its consequences regarding the evolution of D_A .

The fact that our estimates of D_A nicely fit into previous measurements and are also well described by the MMC and MTC models, as can be seen in Figures 2 and 3, supports our assumption that the underlying QSO continuum in the Ly α forest region can be estimated via the extrapolation of the power-law fitted in the region redward of the Ly α emission line. However, we are aware of the fact that we may have systematically overestimated the continuum level, and that our measurements of D_A maybe therefore slightly overestimated as well. This would explain why our measurements are higher on average than the median value of D_A predicted by the MMC model. It is worth mentioning, however, that in contrast to previous models (e.g. Zuo 1993) we explicitly avoid normalising in any way the used distributions to match the observed D_A at some given redshift, or manipulating the models whatsoever to satisfy any other restriction. We simply take the distributions as reported in the literature, where they were determined directly from line statistics by the authors, and references therein. We mention this in order to emphasize even more the excellent agreement between the MMC model and the observations.

5.2 Distribution of D_A

Judging from the dependence of Φ on τ and N_{abs} (see equation 12), it is expected that the transmission factor and consequently D_A are rather complicated random variables. As is well known from statistics, a random variable x that can be expressed as the product of a large number of small, statistically independent factors is distributed lognormally, *i.e.* according to the distribution

$$f(x; \mu, \sigma) = \frac{1}{\sqrt{2\pi\sigma^2}x} e^{-\frac{1}{2}\left(\frac{\ln x - \mu}{\sigma}\right)^2}, \quad (18)$$

where μ and σ are the mean and the standard deviation of $\ln x$. This expression is equivalent to the statement that a random variable x is distributed lognormally, if and only if its logarithm is distributed normally.

The expected value μ' and the standard deviation σ' of a log-normal distributed quantity can be expressed in terms of the parameters μ and σ as

$$\mu' = e^{\mu + \frac{1}{2}\sigma^2}, \quad (19)$$

and

$$\sigma' = (e^{\sigma^2} - 1)^{1/2} \mu'. \quad (20)$$

From the form of equation (12) we may suspect that the transmission factor is a lognormally distributed variable, since it can be expressed as the product of a large number of statistically independent factors that take on values in the range $[0, 1]$. The implications of this statement are profound: if Φ is distributed lognormally, so does $\bar{\Phi}_z$ and consequently $D_A(z)$. Furthermore, due to the property of the lognormal distribution stated above, the effective optical depth of the Ly α absorption, usually defined as $\tau_{eff} \equiv -\ln(1 - D_A)$ (see e.g. Kim, Cristiani & D'Odorico 2001) should obey a Gaussian distribution. This result follows independently from the fact that the total optical depth can be expressed as the sum of the independent contribution of each system, as indicated in equation 12). Thus, for a sufficiently large number of absorbers N_{abs} , and if the optical depth for each absorber has the same mean value $\langle\tau\rangle$ and dispersion $\sigma(\tau)$ at each wavelength, τ_{eff} should obey a Gaussian distribution at each redshift, centered at $N_{abs}\langle\tau\rangle$ and dispersion $\sqrt{N_{abs}}\sigma(\tau)$. The most astonishing fact is that these statements are completely independent of the form of evolution of the intergalactic neutral hydrogen, as long as the transmission factor can be expressed in the form of equation (12). Thus, it should be a fact of nature that the distribution of the absorbed flux at any given wavelength should obey a lognormal distribution.

In order to test whether the values of D_A obey a lognormal distribution, we compute the mean and standard deviation of $\ln D_A$ for the ensemble of $4 \cdot 10^3$ lines-of-sight at a given redshift according to the equations

$$\mu(\ln D_A) \equiv \frac{1}{N_{LOS}} \sum_{i=1}^{N_{LOS}} \ln D_A^i, \quad (21)$$

and

$$\sigma^2(\ln D_A) \equiv \frac{1}{N_{LOS} - 1} \sum_{i=1}^{N_{LOS}} (\ln D_A^i - \langle \ln D_A \rangle)^2, \quad (22)$$

With these parameters, we generate normally distributed random numbers using the Monte Carlo technique, and compare them to the $\ln D_A$ values from our simulations at each given redshift, in order to determine whether the latter are normal distributed. Recall that $\ln D_A$ is distributed normally if and only if

D_A obeys a lognormal probability distribution. As a first approach, we choose to compare both data sets graphically using Quantile–quantile plots (QQ plots for short), and to this end we compute for each set of values the 50 per cent quantile (median), and the ± 34.13 , ± 43.32 , ± 47.72 , ± 49.38 , and ± 49.87 per cent quantiles around the median, as done in previous sections. With this graphical aid it is possible to tell qualitatively if the data sets compared to each other are drawn from the same parent distribution. As a thumb rule, one can say that the closer the quantiles lie to the identity line in a QQ plot, the larger the probability that both data sets obey the same distribution. In order to evaluate this statement quantitatively, we define the following measure

$$\delta^2 \equiv \sum_{i=1}^{N_q} \left(\frac{Q_i - q_i}{Q_i} \right)^2, \quad (23)$$

where the Q 's are the quantiles determined from random numbers distributed normally, the q 's are the corresponding quantiles of the $\ln D_A$ values at a given redshift that result from our simulations, and $N_q = 11$ is the number of quantiles. By definition, δ explicitly gives the absolute deviation of one data set with respect to the other, and hence quantifies the departure of the assumed distribution. Indeed, the smaller the value of δ , the larger the probability that both data sets belong to the same distribution. In Figure 4 we show the QQ-plots at each redshift and together with the corresponding value of δ . As can be judged by visual inspection, the departure of the distribution of $\ln D_A$ from a Gaussian distribution is negligible at all redshifts. Furthermore, the quoted values of δ seem also vanishingly small. However, since the distribution of the random variable δ itself is unknown, we try to determine the significance of the results by generating two sets of normally distributed random numbers with mean and standard deviations distributed uniformly, and comparing them to the values found for our simulated data. We do this for $1.2 \cdot 10^6$ pairs of sets, and determine from these what is the fraction of realisations with a value of δ smaller than a given value. We expect this procedure to quantify the probability that the values of δ quoted in Figure 4 happen by chance. According to these estimates, there is a probability of $\{1.4 \cdot 10^{-2}, 3.1 \cdot 10^{-3}, 1.9 \cdot 10^{-4}, 2.3 \cdot 10^{-5}\}$ that a value $\delta \leq \{0.50, 0.25, 0.10, 0.05\}$ will be produced by chance, respectively. In Figure 6 we show the values for δ as a function of redshift with the MMC model. Note that for the whole redshift range shown, $\delta \lesssim 0.5$, and in particular $\delta \lesssim 0.1$ for $z_{em} > 1.5$. Based on these results, we may conclude that the distribution of $\ln D_A$ at a given redshift is Gaussian with a confidence level of 99 per cent, which implies that D_A obeys a lognormal distribution with the same confidence.

It follows from the Central Limit Theorem that the larger the number of absorbers N_{abs} , the closer the approach of the distribution of Φ to a lognormal distribution. Since N_{abs} increases with redshift, it should be expected that the accuracy with which the distribution of Φ approaches a lognormal distribution also increases with redshift. Furthermore, if the integral in equation (13) is approximated by a sum of the form

$$\bar{\Phi}_z \approx \frac{1}{N} \sum_{i=1}^N \Phi_i \Delta \lambda_i,$$

where N is the number of pixels, it becomes evident that for sufficiently large N , and assuming that Φ has the same mean value $\langle \Phi \rangle$ and dispersion $\sigma(\Phi)$ at each pixel, the distribution of $\bar{\Phi}_z$ should approach a Gaussian distribution with mean $\langle \Phi \rangle$ and dispersion $\sigma(\Phi)/N$. Since the width of a given restframe wavelength range,

i.e. the number of pixels also increases with redshift as $(1+z)$, it is expected that the approximation of the distribution of $\bar{\Phi}_z$ and hence of D_A to a Gaussian becomes better with increasing redshift. We thus have the superposition of two effects: On the one hand, the distribution of Φ at a fixed wavelength approaches a lognormal distribution at all redshifts, with the accuracy increasing with redshift. On the other hand, the distribution of $\bar{\Phi}_z$ and $D_A(z)$ approaches a Gaussian distribution with increasing redshift. The net result should be that $\bar{\Phi}_z$ and D_A are distributed lognormally at low redshifts, and that their distribution approaches a Gaussian for higher redshifts. Since D_A asymptotically converges to unity for very high redshifts, the Gaussian distribution at these redshifts is expected to be highly peaked around its mean value. This is naturally given by the fact that the dispersion of $\bar{\Phi}_z$ scales like $\sigma(\Phi)/N$ around $\langle \Phi \rangle$, as stated above.

We compute the theoretical lognormal probability distribution as given by equation (18) with the mean and standard deviation of $\ln D_A$ computed using equations (21) and (22). We do the same for a Gaussian distribution, using the same equations as before, but replacing $\ln D_A$ by D_A , and compare both these theoretical distributions to the distribution of the D_A values at a given redshift that result from our simulations. This comparison is shown in Figure 5. Note the excellent agreement at all redshifts between the lognormal probability distribution and the distribution of the D_A values resulting from our simulations. We want to emphasize that the theoretical curves shown are not fits to the binned data, but are computed using only the mean and standard deviation of the unbinned data. The data were binned only for display purposes. At lower redshift, the agreement at the lower cut-off, *i.e.* at $D_A = 0$ is worth mentioning. It is remarkable that this cut-off, which is physically given by the fact that D_A cannot take on values smaller than zero, arises in a natural way due solely to the fact that D_A is distributed lognormally. Note, in contrast, that a Gaussian distribution does not satisfactorily describes the distribution of the data at these low redshifts. Nevertheless, the description of the data by Gaussian distribution becomes better with increasing redshift, as previously stated, and the corresponding Gaussian distribution becomes narrower at every increasing redshift. Note also that the theoretical lognormal and Gaussian distribution become visually indistinguishable from each other at high redshifts. In order to assess quantitatively the differences between these distributions with respect to the distribution of the data, we compute again the value of δ at each redshift, assuming now that the values of D_A values obtained from the MMC model are drawn from a Gaussian parent distribution. We compare these values to the corresponding values computed before for an assumed lognormal parent distribution. This comparison is shown in Figure 6. As can be seen, the values of δ for both distributions are low at all redshifts, and the difference between them at $z_{em} \gtrsim 2$ is negligible small. This explains why the lognormal and Gaussian distribution functions shown in Figure 5 are practically indistinguishable from each other. However, note that the values of δ for a assumed Gaussian parent distribution become vanishingly small with increasing redshift, and thus the probability that the data are drawn from this distribution increases with redshift, eventually becoming larger than the corresponding probability for the lognormal distribution. Besides, it can be seen also that the δ values for a assumed lognormal distribution rise again towards high redshifts, implying that the distribution of the data at these redshifts is no longer well described by a lognormal distribution. This confirms our statement made above, that D_A is expected to be distributed lognormally at low redshifts and normally at higher redshifts. The redshift at which the transition from a lognormal to a Gaussian distribution

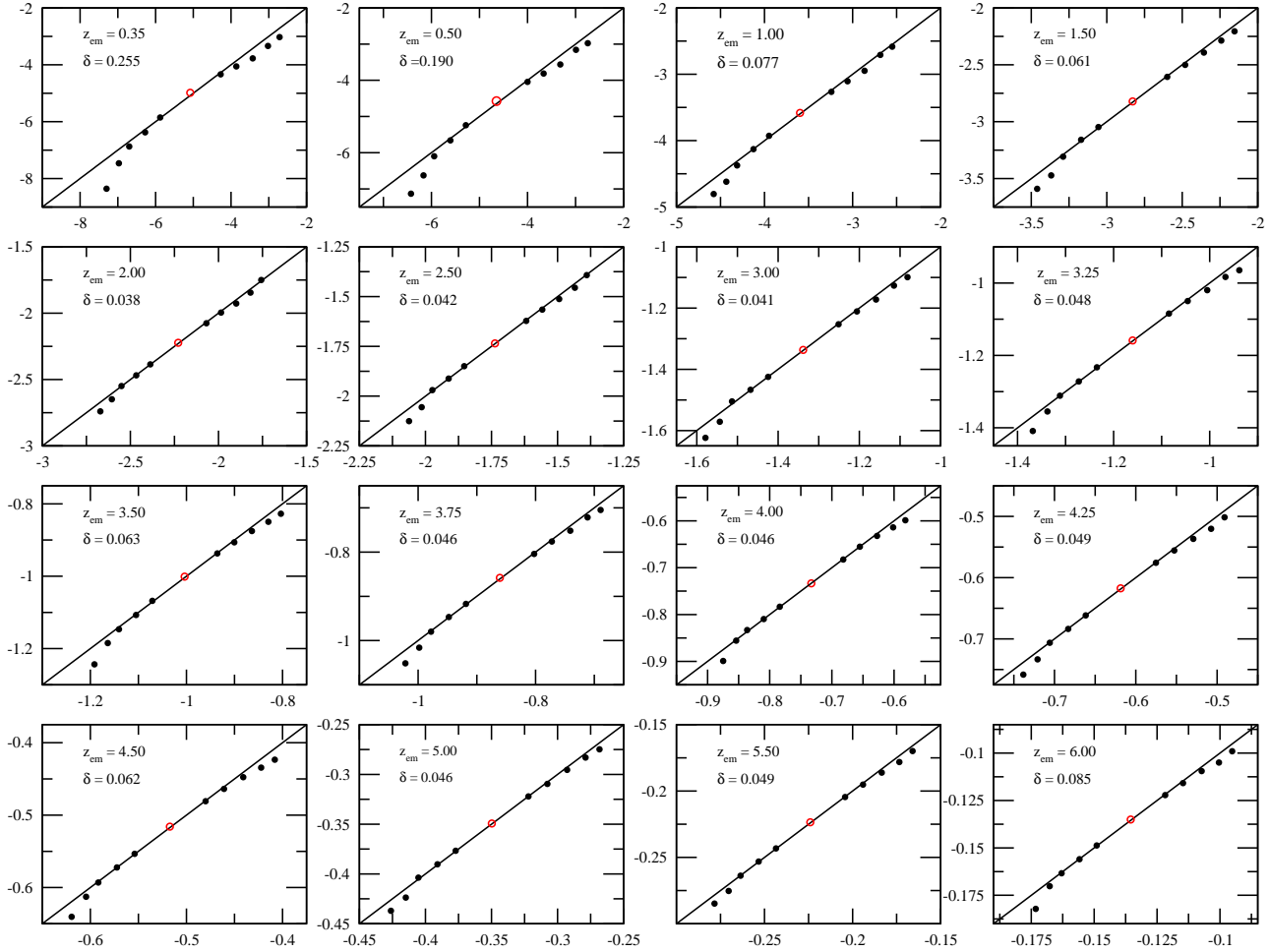


Figure 4. Quantile-quantile Plot for the values of $\ln D_A$ computed from the MMC model. Shown are the quantiles corresponding to the $\pm 1, \pm 1.5, \pm 2, \pm 2.5$ and $\pm 3\sigma$ ranges for the logarithm of our simulated values of D_A and for a realisation of normal deviated random numbers with the same parameters, *i.e.* mean and standard deviation, as the simulated data. An open circle denotes the median, and its nearest neighbouring points the $\pm 1\sigma$ range, the next nearest the $\pm 1.5\sigma$ range, and so on. The solid line represents the ideal case where both data sets are drawn from the same parent distribution. The deviation from this ideal situation is quantified by the parameter δ , which takes on values between 0 (both data sets belong to the same distribution with unit probability), and ∞ (both data sets *do not* belong to the same distribution with unit probability).

takes place may depend on the particular set of input distributions used. For redshifts where the distribution of D_A is well approximated by a lognormal distribution, it is straightforward to see that the optical depth must be distributed normally. This result is not at odds with the results from *e.g.* Madau (1995, Figure 1), Meiksin (2004, Figure B1), or Bernardi et al. (2003, Appendix C).

5.2.1 The Effect of the Lyman limit systems (LLSs)

It is usually assumed that the presence of the high-density Lyman limit systems tends to skew the distributions of the opacity and hence of the absorption towards larger values, making values smaller than the mean more probable (see *e.g.* Madau 1995, Meiksin & White 2004). In order to quantify the effect that the LLSs have on the distribution of D_A , we compare, following the analysis of Section 5.2, the results of the simulations for the MMC model with and without the optically thick LLSs. We find that D_A

is lognormally distributed as well with a high confidence for the case where the LLSs are excluded, as can be seen in Figure 6, where the values for δ computed at each given redshift are shown. Note that the values of δ for the MMC model without LLSs are larger at redshifts $z_{em} \lesssim 3$ than those for the full MMC model. This is due to the fact that the absence of the optically thick LLSs enhances the probability of the attenuation factor $\exp(-\tau)$ to be closer to unity at a given wavelength along a random line-of-sight. This means effectively that the number of factors in equation (12) are reduced. Hence, when the LLSs are absent, the approach to a lognormal distribution should be worse with respect to the case where the LLSs are included. Furthermore, this effect should be enhanced towards lower redshifts, for which the number of factors, *i.e.* of absorbers decreases as $\propto (1 + z_{em})^\gamma$. Note that the trend is the opposite in the case of a assumed Gaussian parent distribution.

We have found when computing the evolution of D_A with the MMC model with and without LLSs that the predictions for the evolution of D_A with redshift for the full MMC model are practi-

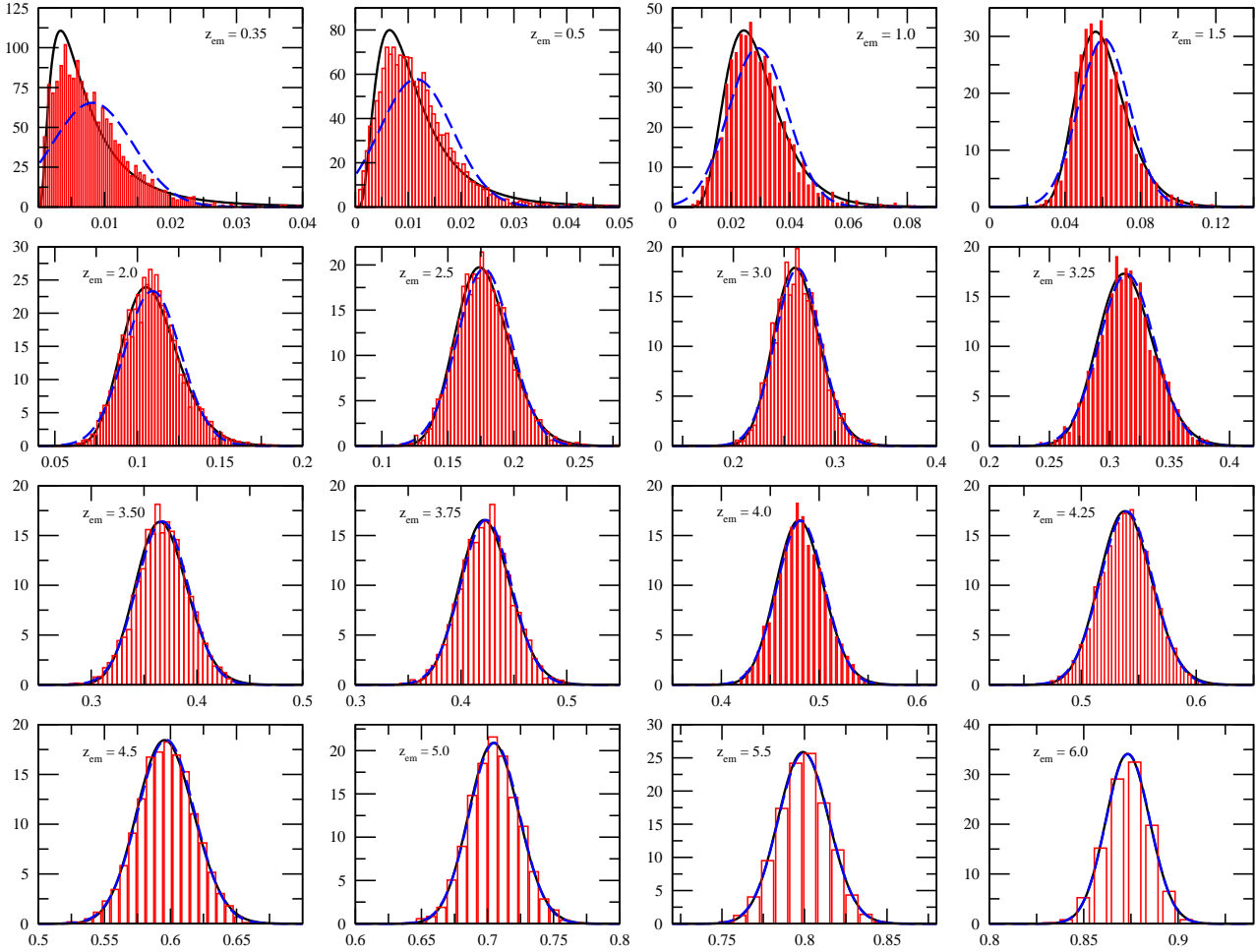


Figure 5. Distribution of the D_A values at a given redshift computed from simulations based on the MMC model (histogram). The distribution is normalised to unit area. Shown are also a theoretical lognormal distribution (solid curve) computed according to equations (18), (21), and (22), and a Gaussian distribution (dashed curve) computed using the same equations as before but replacing $\ln D_A$ by D_A . The y-axis indicates the probability of the corresponding D_A value on the x-axis. The bin size used to compute the histogram at each redshift has been arbitrarily chosen to be given by $\max\{D_A(z)\}/100$, and is hence different at each redshift. However, the binning of the data is intended only for display purposes. The binned data have not been used in any form to estimate the parameters of the corresponding probability distribution. We want to emphasize that the theoretical curves shown are not fits to the binned data, but are computed using only the mean and standard deviation of the unbinned data. Note the excellent agreement between the data and the theoretical lognormal distribution, especially with respect to the skewness and the cut-off at $D_A = 0$. The distribution of the data is not well described by a Gaussian distribution at the lowest redshifts shown. However, the approach of the data distribution to a Gaussian distribution increases with increasing redshift (see text for details).

cally indistinguishable from the results of the MMC model without LLSs, meaning that the effect of these systems on the total absorption is negligible. Furthermore, it turns out that the distribution of D_A values is skewed, *i.e.* it is lognormal irrespective of the presence of LLSs. All these results point to the fact that the LLS have a negligible impact on the evolution of the intergalactic absorption, as long as the input distributions used here correctly describe the number density evolution of the absorbers. This confirms the results from Desjacques, Nusser & Sheth (2007), and the picture shall not be fundamentally different, if higher column density systems such as damped Ly α systems were present, as pointed out by McDonald et al. (2005).

These results certainly demand an explanation. We think that, as long as the distribution functions realistically describe the evolution of the Ly α absorbers, the LLSs *cannot* have a great impact

neither on the absorption, nor on its statistics because of the following reasons: 1) They are scarce, and even more compared to the thinner Ly α forest systems (*e.g.* 5 LLSs on average along a random line-of-sight compared to approximately 1500 Ly α forest absorbers out to $z = 3.0$, according to the MMC model); 2) Their contribution to the absorption is due solely to their Ly α absorption line (not the Lyman break), and the equivalent width of the systems with column densities $N_{\text{HI}} = 10^{17.21-18} \text{ cm}^{-2}$, as can be seen from a curve-of-growth (Figure 7), is not too different from that of the systems with column densities $N_{\text{HI}} = 10^{14-15} \text{ cm}^{-2}$, which are by far more numerous. For example, the input distributions of the MMC model predict that the ratio of the average number of the optically thin Ly α forest absorbers to the number of optically thick Lyman limit systems at a redshift $z_{\text{em}} = 4.0$ amounts to 477. If we suppose that *all* Ly α forest and Lyman limit systems are absorbers with the

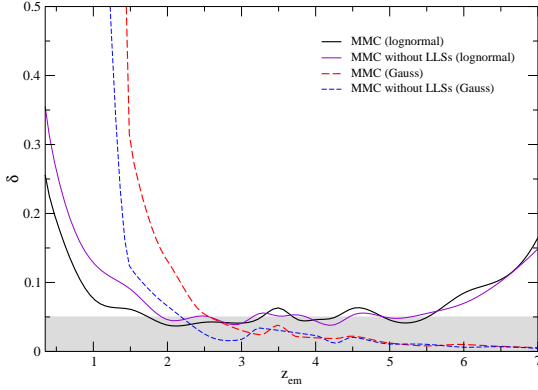


Figure 6. Values of δ for the MMC model assuming a lognormal (heavy solid line) and Gaussian (heavy dashed line) parent distribution. The shaded area indicates the range $\delta \leq 0.05$, that corresponds to a probability of $1.9 \cdot 10^{-5}$ that the data are not drawn from the same parent distribution. Note how the assumption of a Gaussian parent distribution improves with redshift, but that a lognormal distribution is a better assumption for low redshifts. The light solid and dashed lines correspond to the MMC model without Lyman limit systems (see Section 5.2.1). Note that the approximation to a lognormal distribution, is better when these systems are included (see text for discussion). The fluctuations seen with respect to a perfect smooth curve in each case are due to the random nature of the process at each redshift, and are not significant.

largest possible column density for their respective column density ranges, *i.e.* $N_{\text{HI}} \approx 10^{17}$ and $N_{\text{HI}} \approx 10^{20} \text{ cm}^{-2}$, then the ratio of the Ly α equivalent width of the thin systems to that of the thick systems for a mean Doppler parameter of 36 km s^{-1} is approximately 0.12. For the case that we take the lowest column density and more numerous systems to be representative of their respective populations, the ratio of their equivalent widths is approximately 0.006. Even in this case, the *total* equivalent width of the optically thin Ly α forest systems dominates over that of the optically thick LLSs by a factor of $477 \cdot 0.006 = 2.89$, at $z_{\text{em}} = 4.0$. In order to see the relative contribution of each population at a given redshift more precisely, we weight the equivalent width $W(N, b)$ with the column density distribution, and compute the ratio

$$\varrho(z_{\text{em}}; b) \equiv \frac{\langle W \rangle_{\text{Ly}\alpha}}{\langle W \rangle_{\text{LLS}}}, \quad (24)$$

where

$$\langle W \rangle_i \equiv \int_0^{z_{\text{em}}} \int_{N_{\text{min}}}^{N_{\text{max}}} (1+z) \cdot W_0(N, b) f_i(N, z) dN dz, \quad (25)$$

Here, f_i is the distribution function of population $i \in \{\text{Ly}\alpha, \text{LLS}\}$, $W_0(N, b)$ is the rest equivalent width of a Ly α absorption line for a column density N and Doppler parameter b , and N_{min} and N_{max} are the column density limits that define each population, respectively. For a reasonable value for the Doppler parameter of 36 km s^{-1} , and the input distributions of the MMC model, we find that $\varrho \gg 1$ at all redshifts. The result is qualitatively the same for the BMC model. It can be concluded from this that the Ly α forest systems dominate the absorption over the optically thicker Lyman limit systems at all epochs. This explains in the first place why the difference between the predictions for D_A from the MMC model with and without LLSs, is vanishingly small. Also, it is consistent with

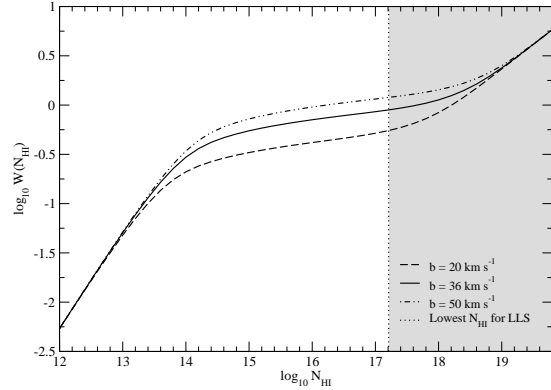


Figure 7. Curve of growth of the Ly α absorption line, for three typical values of the Doppler parameter. The shaded region corresponds to the column densities characteristic to Lyman limit systems.

the fact that the distribution of D_A should not be far from lognormal or Gaussian, with or without LLSs, since this only depends on the fact that the absorption factor be expressed in the form of equation (12), and this is truly independent of the form of the input distributions, as stated previously. Finally, It also explains why the behaviour of $\sigma(D_A)$, as shown in the next section (cf. Figure 8), is qualitatively the same irrespective of the presence of these systems.

We thus conclude that the distribution of D_A , *i.e.* the flux field for a given redshift as predicted by the MMC model, is lognormally distributed with a high confidence at redshifts $z_{\text{em}} \lesssim 6$, and consequently, that $\ln D_A$ and hence the optical depth of H α obey a Gaussian distribution, in disagreement with the results of previous analyses (*e.g.* Madau 1995, Bernardi et al. 2003, Tytler et al. 2004a, Meiksin 2004).

5.3 Scatter in D_A

We expect the intrinsic scatter in the absorption due to cosmic variance to be strongest at lines-of-sight of middle length. At low redshifts, both the number of thin Ly α forest clouds and thick Lyman limit systems is small, and the addition of a few more does not change dramatically the amount of absorption. However, the number of Ly α forest clouds increases rapidly with z , and thus the probability of encountering more or less systems than average increases as well. Correspondingly, the absorption increases and so does its scatter. At even higher redshifts, the number of Ly α forest systems increases so dramatically and the absorption is so severe that the addition of more systems does not make any difference neither to the absorption nor to the scatter. Thus, we should expect the stochastic effect, *i.e.* the scatter in absorption, to peak at some intermediate redshift z_{int} .

We compute the intrinsic scatter at the σ level for the values of D_A at each given redshift obtained from our simulations using equations (19), (20), (21), and (22). The result is shown in Figure 8, where we show the evolution of the scatter in D_A with redshift for the MMC model with and without LLSs. We also include for completeness the result from the BCG model. It can be seen that, irrespective of the model, the scatter peaks at a intermediate redshift

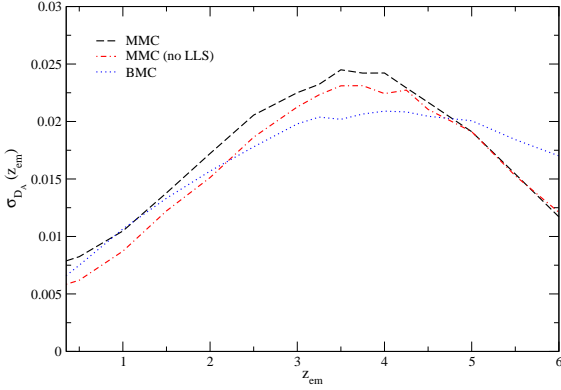


Figure 8. Evolution of the intrinsic scatter of D_A due to the stochastic nature of the absorption in the intergalactic medium for the two competing models MMC (dashed line) and BMC (dotted line). The dot-dashed line corresponds to the MMC without Lyman limit systems (see Section 5.2.1 for details). Note that the behaviour of $\sigma(D_A)$ is qualitatively the same for all three models. As expected, the amount of scatter for the MMC model is less in the case where the Lyman limit systems are absent.

between $z_{em} \approx 3.5$ and $z_{em} \approx 4.0$. Note that the peak is significant, since it represents an increase in the scatter of 2.5 times with respect to its value at $z_{em} \approx 1$. It is interesting that this result had also been found by Zuo (1993, Figure 2), who using a semi-analytic approach and different input distributions, reported that $\sigma(D_A)$ is largest at redshifts near 3.7. Thus, the qualitative behaviour of the intrinsic scatter of D_A shown in Figure 8 may be an unavoidable feature of this observable, which could explain at least in part the large scatter in the measurements of D_A seen in the same redshift interval (cf. Figure 2). As stated above, however, the large scatter in the observations at these redshifts cannot be accounted for by the models, not even at the 3σ level.

When comparing models that only differ by the presence of the optically thick Lyman limit systems, we find that the scatter in D_A is larger at any given redshift when the LLS are present. None the less, the absolute value of the scatter does not differ significantly between the situation where these systems are present and where they are absent. Thus, the contingent presence of a few less or more thicker systems does introduce a variation in the absorption from one line-of-sight to another, even though the absorption itself does not vary in a significant amount. In other words, the net effect of the LLSs is to enlarge the intrinsic scatter in the absorption. However, note that for redshifts $z_{em} \gtrsim 4.0$, the amount of scatter at the 1σ level becomes indistinguishable between both models, owing to the fact that the thinner Ly α forest systems are overwhelmingly numerous at these redshifts.

The results above support our previous conclusion that the optically thick LLSs cannot have a great impact on the absorption and on its scatter. The fact that LLSs (and maybe DLAs) do not have a great impact on the scatter in absorption is even more apparent when assessing their effect on broad-band colors. This is mainly because their Lyman break is *always* blueward of the Lyman break of the source, and their Ly α lines do not contribute significantly to the absorption, especially when integrating the flux over a large wavelength range characteristic of broad-band filters. We leave this analysis to a forthcoming paper.

We want to highlight two curiosities: First, by taking a close look at Figures 3 and 8 it becomes apparent that the maximum in the evolution of $\sigma(D_A)$ roughly coincides with the point of inflection of the curve that describes the redshift evolution of D_A . Mathematically, this implies that the intrinsic scatter of D_A is proportional to the rate of change of D_A with redshift, *i.e.*

$$\sigma(D_A) \propto \frac{\partial D_A}{\partial z}. \quad (26)$$

Indeed, if one computes numerically the derivative of D_A with respect to z , it turns out that it qualitatively matches the evolution of $\sigma(D_A)$, up to a scale transformation. A possible interpretation may be that a stronger evolution of D_A , *i.e.* a stronger change with z (where the rate of change is given by the derivative) implies a rapid change in the evolution of the absorbers. This implies a larger variation in the absorption from line-of-sight to line-of-sight, and thus a larger value of $\sigma(D_A)$.

Second, it is interesting to note that the redshift at which the intrinsic scatter in evolution of D_A peaks roughly coincides with the redshift at which the observations show a strong scatter, *i.e.* around $z_{em} \approx 3.5$. This roughly matches the redshift at which Bernardi et al. (2003) reported a particular feature in the evolution of the Ly α optical depth, which has been interpreted by the authors as a signature of the reionisation of He II. If these is a mere coincidence or if it has a more profound meaning requires further detailed analysis, which is however beyond of the scope of the present work.

6 SUMMARY & CONCLUSIONS

(i) We measured the cosmic flux decrement D_A and its uncertainty for 25 QSOs of the SDSS DR5 catalog in the redshift range $2.71 \leq z_{em} \leq 5.41$.

(ii) We modeled the redshift evolution of D_A in a Monte Carlo fashion, using two different sets of input distributions for the absorber properties, and found that the prediction of the MMC model reproduce well the observations in the range $0.2 < z_{em} < 5.41$, in contrast to the BMC model. We conclude from this that the underlying input distributions of the BMC model do not quite describe the evolution of the Ly α absorption on the IGM, and that previous estimates of the impact of the intergalactic attenuation on the photometric properties of high-redshift galaxies using this model are inaccurate. Incidentally, by comparing the simulations to the data, we show the power of the relatively simple approach used here to model the effect of intergalactic absorption, as compared to models based on hydrodynamical simulations which are by far more complex and yield similar results.

(iii) We found from our simulations that the distribution of the D_A values at a given redshift is well described by a lognormal distribution at low redshifts and even better by a Gaussian distribution at high redshifts, in agreement with the fact that the absorption consists of the product of statistically independent factors. This result implies that at redshifts where D_A is distributed lognormally, the effective optical depth of the intergalactic H I obeys a normal distribution, contrary to the results of previous studies. However, a larger number of accurate measurements are needed to determine whether D_A is truly distributed (log-)normally. We leave as an open question whether the result that D_A is distributed lognormally is linked in some way to the assumption that the primordial density fluctuations that gave origin to the structure formation in the Universe, and that ultimately gave rise to the Ly α absorbers, obey a lognormal distribution as well, as proposed by Bi, Boerner & Chu (1992).

(iv) We conclude that the optically thick Lyman limit systems have a negligible effect on the absorption, even though they do increase its intrinsic scatter. As expected on a theoretical basis, the presence of these systems does not significantly affect the distribution of D_A . These results are subject to the assumption that the evolution of these systems is given by the input distributions used.

ACKNOWLEDGMENTS

We are grateful to Avery Meiksin for computing a special set of tables of his transmission functions. We also want to thank Nico Bissantz for useful suggestions about the statistical treatment of the data. TTG acknowledges financial support from the Mexican Council for Science and Technology (CONACyT).

Funding for the SDSS and SDSS-II has been provided by the Alfred P. Sloan Foundation, the Participating Institutions, the National Science Foundation, the U.S. Department of Energy, the National Aeronautics and Space Administration, the Japanese Monbukagakusho, the Max Planck Society, and the Higher Education Funding Council for England⁵.

The SDSS is managed by the Astrophysical Research Consortium for the participating Institutions. The Participating Institutions are the American Museum of Natural History, Astrophysical Institute Potsdam, University of Basel, University of Cambridge, Case Western Reserve University, University of Chicago, Drexel University, Fermilab, the Institute for Advanced Study, the Japan Participation Group, Johns Hopkins University, the Joint Institute for Nuclear Astrophysics, the Kavli Institute for Particle Astrophysics and Cosmology, the Korean Scientist Group, the Chinese Academy of Sciences (LAMOST), Los Alamos National Laboratory, the Max-Planck-Institute for Astronomy (MPIA), the Max-Planck-Institute for Astrophysics (MPA), New Mexico State University, Ohio State University, University of Pittsburgh, University of Portsmouth, Princeton University, the United States Naval Observatory, and the University of Washington.

REFERENCES

- Bernardi M. et al., 2003, *AJ*, 125, 32
 Bershadsky M. A., Charlton J. C., Geoffroy J. M., 1999, *ApJ*, 518, 103
 Bi H. G., Boerner G., Chu Y., 1992, *A&A*, 266, 1
 Bicker J., Fritze-v. Alvensleben U., Möller C. S., Fricke K. J., 2004, *A&A*, 413, 37
 Cristiani S., Giallongo E., Buson L. M., Gouiffes C., La Franca F., 1993, *A&A*, 268, 86
 Desjacques V., Nusser A., Sheth R. K., 2007, *MNRAS*, 374, 206
 Dobrzycki A., Bechtold J., 1991, *ApJ*, 377, L69
 Duncan R. C., Ostriker J. P., Bajtlik S., 1989, *ApJ*, 345, 39
 Fan X., Narayanan V. K., Strauss M. A., White R. L., Becker R. H., Pentericci L., Rix H.-W., 2002, *AJ*, 123, 1247
 Giallongo E., Cristiani S., Trevese D., 1992, *ApJ*, 398, L9
 Giallongo E., D’Odorico S., Fontana A., McMahon R. G., Savaglio S., Cristiani S., Molaro P., Trevese D., 1994, *ApJ*, 425, L1
 Giallongo E., Gratton R., Trevese D., 1990, *MNRAS*, 244, 450
 Gunn J. E., Peterson B. A., 1965, *ApJ*, 142, 1633
 Jenkins E. B., Ostriker J. P., 1991, *ApJ*, 376, 33
 Karzas W. J., Latter R., 1961, *ApJS*, 6, 167
 Kim T.-S., Cristiani S., D’Odorico S., 2001, *A&A*, 373, 757
 Kim T.-S., Hu E. M., Cowie L. L., Songaila A., 1997, *AJ*, 114, 1
 Kirkman D., Tytler D., Lubin D., Charlton J., 2007, *MNRAS*, pp 131–+
 Kirkman D. et al., 2005, *MNRAS*, 360, 1373
 Kirkman D., Tytler D., Suzuki N., O’Meara J. M., Lubin D., 2003, *ApJS*, 149, 1
 Lamb D. Q., Reichart D. E., 2000, *ApJ*, 536, 1
 Laor A., Fiore F., Elvis M., Wilkes B. J., McDowell J. C., 1997, *ApJ*, 477, 93
 Lu L., Sargent W. L. W., Womble D. S., Takada-Hidai M., 1996, *ApJ*, 472, 509
 Lynds R., 1971, *ApJ*, 164, L73+
 Madau P., 1995, *ApJ*, 441, 18
 McDonald P., Seljak U., Cen R., Bode P., Ostriker J. P., 2005, *MNRAS*, 360, 1471
 Meiksin A., 2006, *MNRAS*, 365, 807
 Meiksin A., White M., 2004, *MNRAS*, 350, 1107
 Møller P., Jakobsen P., 1990, *A&A*, 228, 299
 Neugebauer G., Oke J. B., Becklin E. E., Matthews K., 1979, *ApJ*, 230, 79
 O’Brien P. T., Wilson R., Gondhalekar P. M., 1988, *MNRAS*, 233, 801
 Oke J. B., Korycansky D. G., 1982, *ApJ*, 255, 11
 Ostriker J. P., Bajtlik S., Duncan R. C., 1988, *ApJ*, 327, L35
 Ostriker J. P., Ikeuchi S., 1983, *ApJ*, 268, L63
 Pierre M., Shaver P. A., Iovino A., 1988, *A&A*, 197, L3
 Rauch M., 1998, *ARA&A*, 36, 267
 Rauch M., Carswell R. F., Chaffee F. H., Foltz C. B., Webb J. K., Weymann R. J., Bechtold J., Green R. F., 1992, *ApJ*, 390, 387
 Rauch M. et al., 1997, *ApJ*, 489, 7
 Sargent W. L. W., Young P. J., Boksenberg A., Tytler D., 1980, *ApJS*, 42, 41
 Schneider D. P., Schmidt M., Gunn J. E., 1989, *AJ*, 98, 1951
 Schneider D. P., Schmidt M., Gunn J. E., 1991, *AJ*, 101, 2004
 Springel V. et al., 2005, *Nature*, 435, 629
 Steidel C. C., Sargent W. L. W., 1987a, *ApJ*, 318, L11
 Steidel C. C., Sargent W. L. W., 1987b, *ApJ*, 313, 171
 Tepper García T., 2006, *MNRAS*, 369, 2025
 Tytler D. et al., 2004a, *ApJ*, 617, 1
 Tytler D., O’Meara J. M., Suzuki N., Kirkman D., Lubin D., Orin A., 2004b, *AJ*, 128, 1058
 Vanden Berk D. E. et al., 2001, *AJ*, 122, 549
 Williams P., Shu C.-G., Ménard B., eds., 2005, *Probing Galaxies through Quasar Absorption Lines*
 Wolfe A. M., Gawiser E., Prochaska J. X., 2005, *ARA&A*, 43, 861
 Zhang Y., Anninos P., Norman M. L., Meiksin A., 1997, *ApJ*, 485, 496
 Zheng W., Kriss G. A., Telfer R. C., Grimes J. P., Davidsen A. F., 1997, *ApJ*, 475, 469
 Zuo L., 1993, *A&A*, 278, 343
 Zuo L., Lu L., 1993, *ApJ*, 418, 601

⁵ The SDSS Web Site is <http://www.sdss.org/>.